

## Influence of electrolytic hydrogenation on stress-corrosion cracking of X70 steel and pipes of long-term exploited main gas pipeline

<sup>1</sup>L. I. Nyrkova\*, <sup>1</sup>A. V. Klymenko, <sup>1</sup>L. V. Goncharenko, <sup>1</sup>S. O. Osadchuk,  
<sup>1</sup>S. Yu. Kovalenko, <sup>1</sup>Yu. O. Kharchenko, <sup>2</sup>V. V. Lavrenyuk

<sup>1</sup>E. O. Paton Electric Welding Institute of the National Academy of Sciences of Ukraine;  
11, Kazymyr Malevych St., Kyiv, 03150, Ukraine

<sup>2</sup>Kyiv National University of Technology and Design;  
2, Mala Shyianovska (Nemyrovycha-Danchenka) St., Kyiv, 01011, Ukraine

Received: 15.04.2023 Accepted: 25.04.2023

### Abstract

Cathodic polarization, which is used in the complex anti-corrosion protection of main gas pipelines to reduce the corrosion rate to a technically acceptable level, causes the decomposition of the soil electrolyte with the recovery of hydrogen, and its penetration into the steel under the action of tensile stresses contributes to the change in the mechanical properties of the pipes and resistance to stress-corrosion cracking. Comprehensive studies were conducted, and the effect of electrolytic hydrogen penetration on stress-corrosion cracking of X70 steel specimens made from a steel sheet and pipe of a long-term main gas pipeline in a model soil electrolyte NS4 under cathodic polarization in the range of potentials from -0.75 to -1.05 V was determined. The following methods were used in the work: slow strain rate tests, potentiometry, voltammetry, electrolytic hydrogenation, the method of scanning electron microscopy, and optical microscopy. It was established that for both types of specimens, the concentration of hydrogen penetrating into the steel during cathodic polarization increases non-monotonically, with a potential shift from -0.75 to -1.05 V. It is noted that the hydrogenation of specimens of steel under investigation begins at a lower protective potential than steel sheet specimens: -0.95 and -1.05 V, respectively. The concentration of hydrogen diffusing into steel for specimens from a sheet changes in the range  $0 \rightarrow 0 \rightarrow 0.057 \text{ mol/m}^3$ , for specimens from an operated pipe  $0 \rightarrow 0.019 \rightarrow 0.024 \text{ mol/m}^3$ . As a result of the course of the hydrogen diffusion process, there is an increase in the susceptibility to stress-corrosion cracking of specimens from the operated pipe compared to specimens from sheet steel. The coefficient of susceptibility to stress-corrosion cracking  $K_S$  for the steel sheet changes less intensively than for the specimens from the operated pipe:  $1.06 \rightarrow 1.06 \rightarrow 1.18$  and  $1.25 \rightarrow 1.35 \rightarrow 1.53$ , respectively. Therefore, it was established that specimens made from long-term operating under complex anti-corrosion protection of the main gas pipeline have an increased susceptibility to electrolytic hydrogenation compared to specimens made of steel sheet, and as a result, an increased susceptibility to stress-corrosion cracking.

**Keywords:** electrolytic hydrogenation, potentiometry, scanning electron microscopy, slow strain rate test, stress-corrosion cracking.

### Formulation of the problem

Most of the main gas pipelines in the territory of Ukraine were built in the second half of the 20th century. Operation in the conditions of complex anti-corrosion protection ensures their efficiency and reliability, but under the influence of mechanical and corrosion factors, the development of unfavorable processes that can lead to destruction is inevitable [1, 2]. Cathodic polarization, which is one of the necessary conditions for anti-corrosion protection, causes the decomposition of the soil electrolyte with the recovery of hydrogen, and its penetration into the steel in the event of disbondment of the protective coating under tensile stresses contributes to the change in the

mechanical properties of pipes [3–6] and resistance to stress-corrosion cracking [7]. The relationship between hydrogen penetration and the properties of pipe steels is complex [8], and there is no data on the effect of hydrogen on the stress-corrosion cracking of new and exploited pipe steels. Therefore, the study of the effect of electrolytic hydrogenation on new and used pipe steels is an important scientific and practical task.

### Analysis of recent research and publications

Stress-corrosion cracking caused by hydrogen occurs under the conditions of a stressed state [9–11]. In works [12, 13], the degradation of pipeline surfaces under the influence of mechanical and corrosive factors and the degradation of the material "in the volume" were investigated. The works of the E.O. Paton Electric Welding Institute [14–17] assessed the condition of the X70 pipes' metal after prolonged operation and storage and found that according to some indicators of the mechanical properties the metal of these pipes did not meet the requirements of regulatory documents, but due

\* Corresponding author:  
lnyrkova@gmail.com

© 2023, Ivano-Frankivsk National Technical  
University of Oil and Gas.  
All rights reserved.

to the high impact viscosity of the metal in its initial state, which was preserved even after long term operation, the condition of the metal can be considered satisfactory.

Works [12, 13, 18] show that stress-corrosion cracking of X52 and X60 steels in the initial state in a corrosive environment occurs along the boundaries of the ferrite and pearlite grains with the formation of deep secondary intergranular cracks and the delamination of ferrite and cementite inside the pearlite grains. According to the authors, destruction by this mechanism begins near the specimens' outer surface, indicating the key role of hydrogen in cracking. It is believed [19] that hydrogen atoms are easily separated at the ferrite/pearlite interface even without external loads. During rapid deformation, hydrogen penetrates pearlite and interacts with its internal vacancies, which leads to transgranular fracture, which begins with pearlite. At slow deformation, the ferrite/pearlite interface is more vulnerable to hydrogen degradation, which leads to intergranular cracks and an increased tendency to form secondary cracks.

Some authors point out that the long-term operation of gas pipelines leads to a slight decrease in the strength limit, yield strength, and a noticeable increase in the relative elongation of low-alloy steels [20–22], as well as a shift of the corrosion potential of the exploited pipe by 20–30 mV to negatively values compared with the stock pipe. It is emphasized that the higher the strength level of steel is, the less its characteristics change. It is shown that the plasticity indicators of X70 steel practically do not change, and those of X60 decrease due to the structural features of the steel.

Deterioration of the properties of the metal of the operated main gas pipeline was revealed by the authors [23] by the drop in impact viscosity, decrease in relative narrowing, and increase in hardness; the plasticity parameters of the metal changed in the opposite way. This is explained by the intensive development of defects at the micro- and sub-micro levels during long-term operation, which is confirmed by fractographic analysis.

Therefore, the results available in the literature contain data on the effect of long-term operation, mainly on the mechanical properties of steels. There is a lack of comparative data on the effects of electrolytic hydrogenation on new and in-service pipe steels.

### Task setting

One of the common causes of accidents on underground main gas pipelines in all countries without exception is stress-corrosion cracking [1, 24]. Considering the relevance of the issue of stress-corrosion cracking of main gas pipelines in the territory of Ukraine, the purpose of the work was to study the effect of electrolytic hydrogenation on stress-corrosion cracking of pipe steel in different states – steel sheet and pipe of a long-term operated main gas pipeline. The work is a part of research conducted with the aim of accumulating data on the susceptibility of steels in different states (sheet, new, long-term service pipes, and

emergency stock pipes) to stress-corrosion cracking. To achieve the goal, the following tasks have been formulated to:

- investigate the susceptibility to electrolytic hydrogenation of specimens of steel sheet and pipe of the long-term operated main gas pipeline made of X70 steel;

- establish how the potential changes at zero current after electrolytic hydrogenation;

- determine the electrochemical properties of the specimens after investigation;

- determine the range of changes of stress-corrosion cracking mechanism of the above specimens;

- investigate the susceptibility to stress-corrosion cracking of specimens of steel sheet and pipe of the operated main gas pipeline made of X70 steel;

- compare the susceptibility to stress-corrosion cracking and electrolytic hydrogenation of specimens of steel sheet and pipe of the main gas pipeline made of X70 steel.

### Presenting of the main material

**Methods and materials.** Specimens for research were made from a steel sheet with a thickness of 16.5 mm and a pipe of a long-term operated main gas pipeline with a thickness of 15.7 mm across the rolling. Their chemical composition and mechanical properties are given in Tables 1, 2.

Working solution – model soil electrolyte NS4 of the composition: 0.122 g/l KCl + 0.483 g/l NaHCO<sub>3</sub> + 0.181 g/l CaCl<sub>2</sub> + 0.131 g/l MgSO<sub>4</sub>, pH 8.2 [26].

Polarization curves were measured on an MTech PGP-550F potentiostat with potential sweep rates of 0.5 and 100 mV/s. Polarization curves were presented in semi-logarithmic coordinates,  $E - \log(i)$ . Current density is given in A/m<sup>2</sup>.

Research of electrolytic hydrogenation of steel was carried out according to [27]. A laboratory setup with an electrochemical cell was used for research. An electrochemical cell has two separate chambers: an oxidation (anode) and an hydrogenation (cathode) chamber. An auxiliary electrode and a reference electrode are located in each chamber. The working electrode made of the studied steel was placed between these chambers. Each set of three electrodes (working, auxiliary, and reference electrodes) was connected to two PI-50-1.1 potentiostats with PR-8 programmers that work independently of each other. In the oxidation chamber, an anodic potential was set on the working electrode; after reaching its constant value, NS4 solution was introduced into the hydrogenation chamber, and polarization potentials of -0.75, -0.95, and -1.05 V were set (relative to the silver chloride reference electrode, s.c.e.). The entire oxidation current was monitored, including the background current, which was usually equal to the polarization current, until its values stabilized. The delay time for the release of hydrogen from the specimen was recorded, that is, the time of hydrogen saturation. A solution of 0.1 M NaOH was used in the anode chamber, and model soil electrolyte NS4 was used in the cathode chamber. The duration of hydrogenation was set equal to 60 minutes.

Table 1 – Chemical composition of the steels under investigation

Specimen characteristic	Mass part of the elements, %								
	C	Mn	Si	S	P	V	Mo	Al	Nb
Sheet	0.096	1.71	0.208	0.009	0.007	0.060	0.03	0.035	0.052
Exploited pipe	0.090	1.39	0.400	0.006	0.023	0.071	<0.01	0.021	0.029
Requirements of B&R 14-3-995 [25]	0.120	1.70	0.500	0.010	0.020	0.080	0.30	0.050	0.060

Table 2 – Mechanical properties of the investigated steels

Specimen characteristic	$\sigma_{0.2}$ , MPa	$\sigma_B$ , MPa	$\delta$ , %
Sheet	440.0	590.0	20.0
Exploited pipe	491.4	588.3	18.7
Requirements of B&R 14-3-995 [25]	441.0	588.0	20.0

The concentration of hydrogen penetrating the surface layer was calculated using the formula:

$$C_0 = \frac{I_{st} L}{D_{ef} F S}, \quad (1)$$

where  $I_{st}$  is the current strength in the stationary regime of hydrogen penetration, A;  $S$  is the specimen square,  $m^2$ ;  $F$  is the Faraday constant (96485 K/mol);  $D_{ef}$  is the coefficient of effective diffusion of hydrogen in steel ( $1.5 \cdot 10^{-9} \text{ cm}^2/\text{s}$ );  $C_0$  is the concentration of hydrogen penetrating through steel membrane,  $\text{mol}/\text{m}^3$ ;  $L$  is the specimen thickness, m.

According to GOST 9.915 the coefficient of effective diffusion of hydrogen in steel, based on the time for fulfillment the condition  $J(t)/J_{st} = 0.63$ , was calculated by the formula:

$$D_{ef} = \frac{L^2}{6t_{0.63}}, \quad (2)$$

where  $t_{0.63}$  is the time to reach the value  $J(t)/J_{st} = 0.63$ .

$$I_{st} = I_{H_2} - I_B, \quad (3)$$

$I_{H_2}$  is the current strength due to hydrogen penetration, A;  $I_B$  is the background current corresponding to the passivation current of the specimen, A.

A sketch of the specimen for corrosion-mechanical tests is shown in Figure 1.

The tests were carried out in air and in solution by stretching the specimens at a speed of  $10^{-6} \text{ s}^{-1}$  on an AIMA-5-1 tensile machine.

Corrosion-mechanical tests were carried out with periodic wetting with a solution according to a cycle of 50 minutes in the solution and 10 minutes in the air at the same polarization potentials as for hydrogenation.

The susceptibility of steel to stress-corrosion cracking was estimated by the dimensionless coefficient, according to the previously developed method [2], where, is the relative narrowing of specimens in air and solution, respectively.

### Research results

The microstructure of the steel sheet is a dispersed ferrite-pearlite mixture with grain elongation in the rolling direction (Fig. 2, a). The size of the ferrite grain is 7–10  $\mu\text{m}$  according to [29]; the banding of the metal corresponds to (3–4) score, series B according to [29]. The microstructure of the metal of the operated pipe is a mixture of ferrite and pearlite (Fig. 2, b). The strips of the pearlite component are discontinuous, the amount of pearlite is no more than 10 %, and the pearlite components are mainly located on the boundaries of the ferrite grains. The size of the ferrite grain is 10–20  $\mu\text{m}$  according to the DSTU 8972 [29], and the banding corresponds to score 2 [28].

**Electrochemical research.** The corrosion potential of X70 steel sheet specimen in the NS4 solution is -0.780 mV, the operated pipe is 40 mV positively, -0.740 V (Fig. 3, a). The anodic slopes are equal to 0.036 and 0.063 V. The limiting diffusion current of

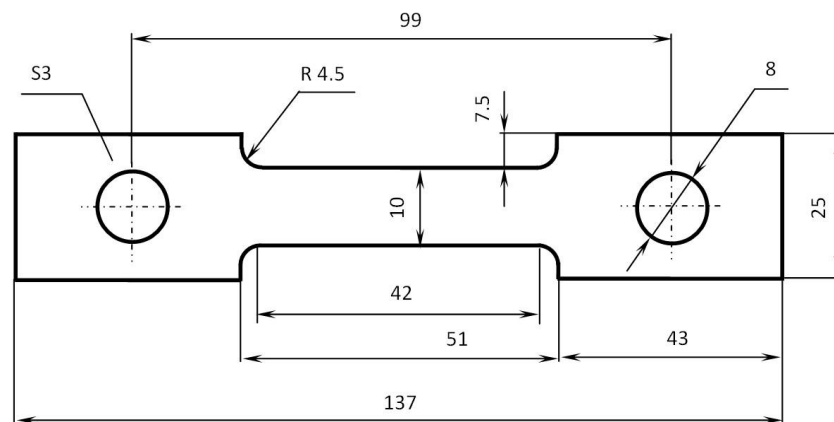
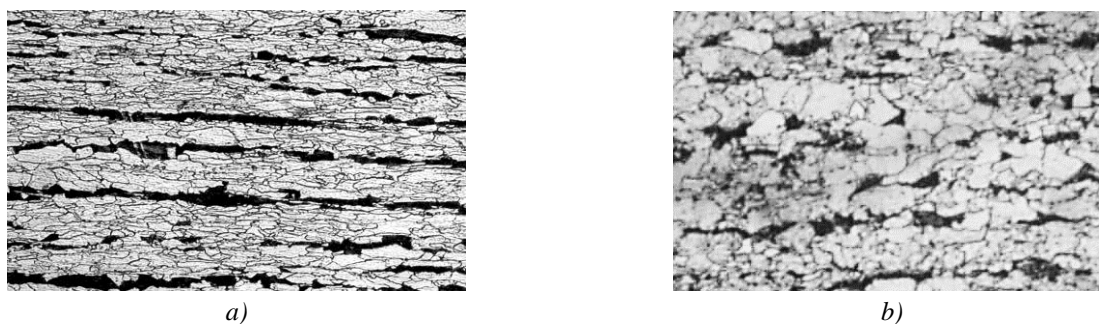
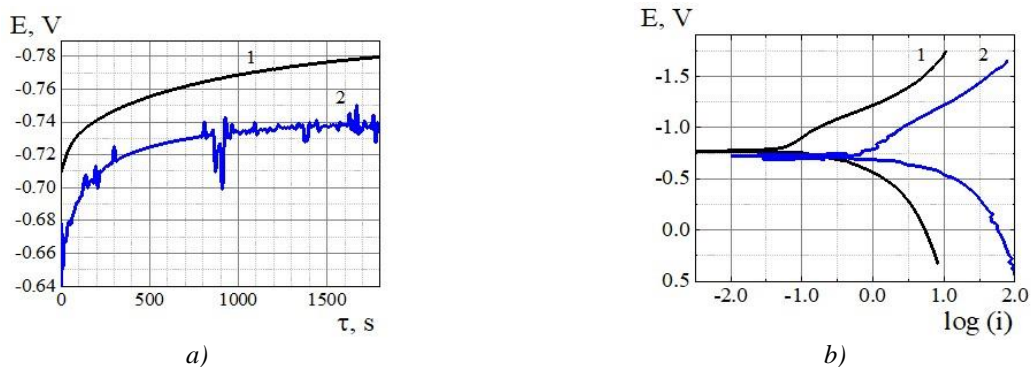


Figure 1 – Sketch of a specimen for corrosion-mechanical tests by slow strain rate method



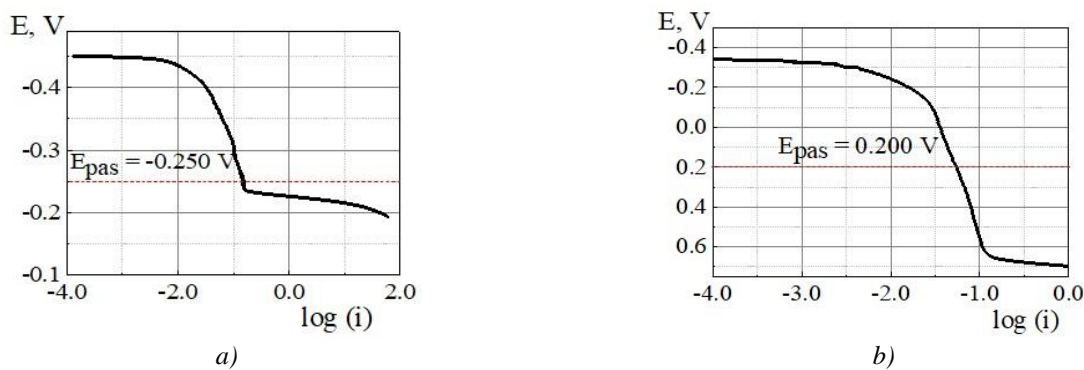
a – steel sheet specimen; b – a specimen of a long-term operated pipe,  $\times 320$

**Figure 2 – Microstructure of the specimens**



1 – steel sheet specimen; 2 – a specimen of a long-term operated pipe

**Figure 3 – Corrosion potentials (a) and polarization curves (b) of X70 steel in NS4 solution**



a – steel sheet specimen; b – a specimen of a long-term operated pipe

**Figure 4 – Anodic polarization curves on X70 steel specimens in 0.1 M NaOH and passivation potentials in the oxidation chamber**

oxygen reduction is  $0.128$  and  $1.69 \text{ A/m}^2$  for specimens from a sheet and an operated pipe, respectively (Fig. 3, b). Lower values of the limiting diffusion current indicate a lower rate of corrosion of sheet specimens. The corrosion rate determined from the polarization curves is  $0.033$  and  $0.01 \text{ A/m}^2$ , respectively.

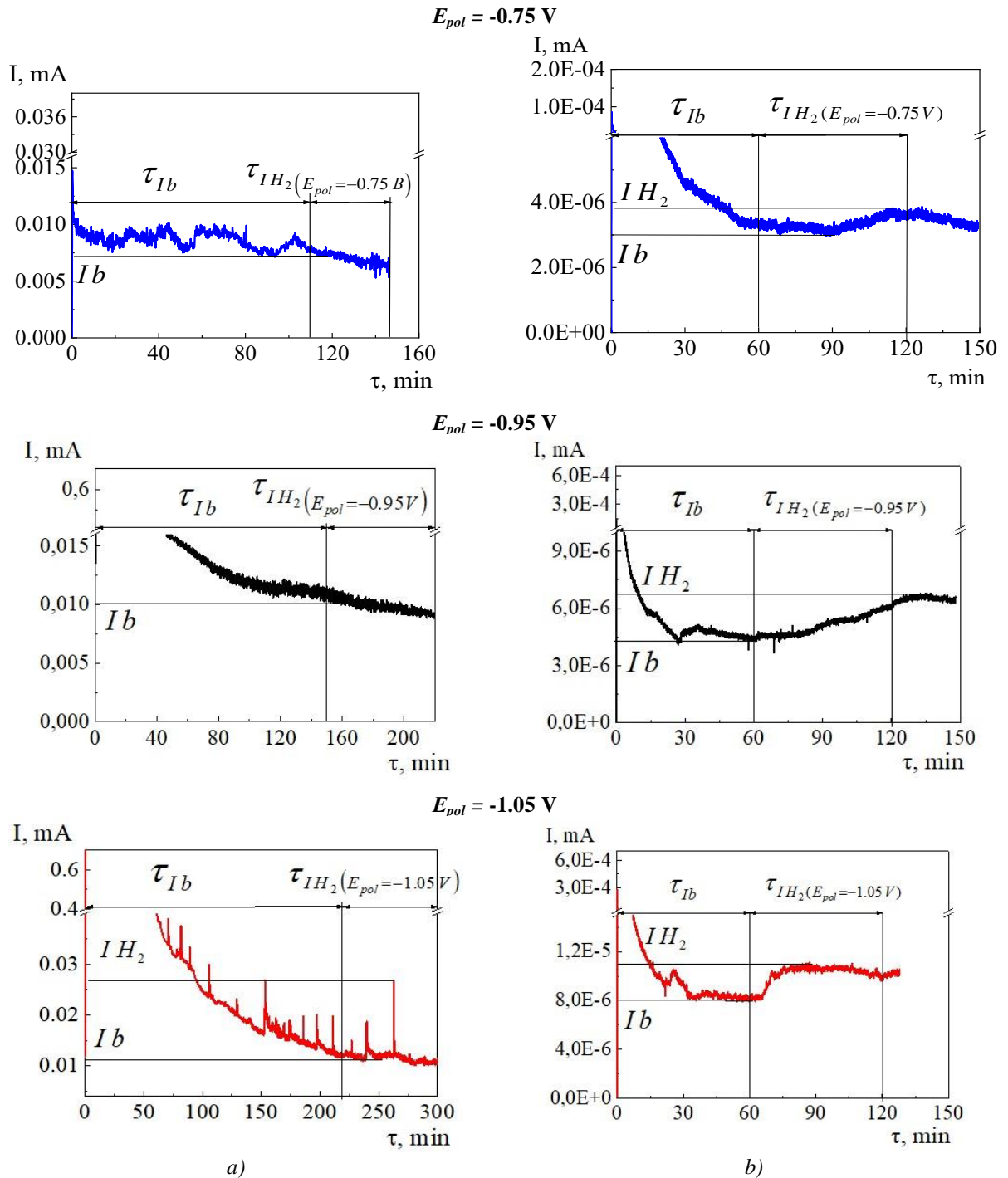
**Research on electrolytic hydrogenation.**

Electrolytic hydrogenation of steels was studied at passivation potentials determined from the region of stable passivation from the anodic polarization curves (Fig. 4), which were set on the anodic side of the steel specimen, respectively  $-0.250 \text{ V}$  for the steel sheet and  $0.2 \text{ V}$  for the operated pipe.

At a polarization potential of  $-0.75 \text{ V}$  (Fig. 5, a) on the steel surface (both for sheet specimens and for the

operated pipe) from the side of the oxidation chamber, the value of the background currents continued to decrease throughout the measurement time. This indicated that at such potentials, hydrogen does not penetrate through steel.

For sheet specimens, the increase in current in the anode chamber began at the potential  $-0.95 \text{ V}$  (Fig. 5, a). The steady-state hydrogenation current was  $3.3 \cdot 10^{-6} \text{ A}$ , the hydrogen concentration on the oxidizing side was equal to  $0.023 \text{ mol/m}^3$ , and the hydrogen release delay time was  $10 \text{ min}$ . At a polarization potential of  $-1.05 \text{ V}$ , when the background current value was set, a jump-like increase in the hydrogen penetration current was observed; the current values were  $0.0079$  and  $0.0160 \text{ mA}$ . The concentrations of hydrogen on the surface of the specimen in the oxidation chamber



a) – steel sheet specimen; b) – a specimen of a long-term operated pipe

**Figure 5 – Current change on X70 steel in the oxidation chamber**

corresponding to these currents were 0.057 and 0.114 mol/m<sup>3</sup>.

For specimens from the operated pipe at a potential of -0.95 V, the increase in current relative to the background value was  $2.51 \cdot 10^{-6}$  A (Fig. 5, b), which corresponded to a hydrogen concentration of 0.0191 mol/m<sup>3</sup>. The hydrogen release delay time was 25 minutes. At a potential of -1.05 V (Fig. 5, b), the hydrogenation current increased to  $3.17 \cdot 10^{-6}$  A, which corresponded to a hydrogen concentration of 0.0241 mol/m<sup>3</sup>. The delay time of hydrogen release was equal to 6 minutes.

It was found that for both types of specimens, the concentration of hydrogen penetrating into steel during cathodic polarization increases non-monotonically with a potential shift from -0.75 to -1.05 V. It was noted that the hydrogenation of specimens of exploited steel begins at a lower cathodic polarization potential than that of steel sheet specimens: at -0.95 and -1.05 V, respectively. The concentration of hydrogen diffusing into steel for sheet specimens varies in the range  $0 \rightarrow 0 \rightarrow 0.057$  mol/m<sup>3</sup> [31], for specimens from an operated pipe –  $0 \rightarrow 0.019 \rightarrow 0.024$  mol/m<sup>3</sup>.

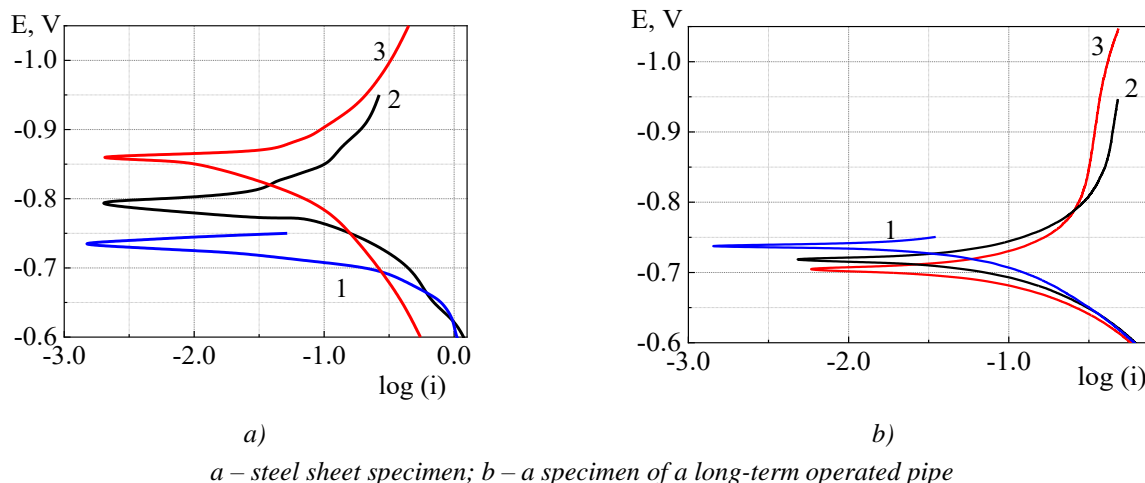


**Figure 6 – Polarization curves on X70 steel after electrolytic hydrogenation tests at cathodic polarization potentials of -0.75 V (1), -0.95 V (2), and -1.05 V (3). Scanning potential rate 0.5 mV/s**

After electrolytic hydrogenation, the electrochemical properties and susceptibility to stress-corrosion cracking of specimens of both types change, in particular, the potential at zero current, determined from the polarization curves (Fig. 6). Therefore, when the cathode polarization potential increases in the series -0.75 V → -0.95 V → -1.05 V for sheet steel specimens, the potential at zero current changes in the sequence -0.735 V → -0.792 V → -0.862 V, and for specimens of the operated pipe -0.738 V → -0.719 V → -0.704 V (Table 3). It has been suggested that in a case of steel sheet, hydrogen formed during cathodic polarization remains in solution near the surface and does not diffuse into the steel, causing embrittlement of its near-surface layer, which contributes to a shift to more negative potential values at zero current. In the case of the specimens from the operated pipe, part of the formed hydrogen diffused into the steel, so the potential at zero current acquired more positive values than for the above-mentioned specimens.

**Table 3 – Null current potential change of the investigated steel specimens after hydrogenation**

Polarization potential during hydrogenation, V	Null current potential, V	
	Steel sheet	Exploited pipe
-0.75	-0.735	-0.738
-0.95	-0.792	-0.719
-1.05	-0.862	-0.704

**Voltammetric determination of the stress-corrosion cracking mechanism.** According to the literature data [31], during the development of stress-corrosion cracking of steel, the tip of the crack is always in an active electrochemical state. On the contrary, the walls of the crack are covered with layers of corrosion products, which is the result of an electrochemical reaction in a quasi-stable state. The difference in the electrochemical states at the top of the crack and the crack wall is the cause of the joint effect of hydrogen

and anodic dissolution on the process of stress-corrosion cracking.

As a new crack is forming, the electrolyte immediately penetrates inside its top, and the induced potential begins to charge the electric double layer and cathodically polarize the surface. It is believed that the cathodic polarization at the top of the crack is lower than outside the crack, which is uniformly polarized when the cathodic potential is applied.

In [31], a theoretical model was proposed, according to which the state at the top of a crack during stress-corrosion cracking development can be simulated on a freshly cleaned metal surface in a corrosive environment by comparing polarization curves taken with slow and fast potential rate speeds. The curve with a high scanning potential rate reflects the electrochemical features at the crack top; the curve with a slow scanning potential rate reflects the electrochemical state of the steel on the surface without a crack (flat surface or crack banks).

Usually, the null current potential of the curve at slow potential scan is positively than in a fast potential scan one, indicating a greater probability of an electrochemical reaction occurring at the crack tip than at the surface area outside the crack due to the difference in polarization potentials. Polarization curves with low and high scan potential rates were obtained and analyzed (Fig. 7). Based on the null current potentials values  $E_0$ , the areas in which the mechanism of stress-corrosion cracking of X70 steel from the sheet and the operated pipe, changes was determined.

It was established that the null current potentials for specimens of a sheet and an operated pipe are equal to  $E_{i=0}^1 = -0.75$  V and  $E_{i=0}^2 = -1.05$  V,  $E_{i=0}^1 = -0.87$  V and  $E_{i=0}^2 = -0.99$  V, respectively (Fig. 7). Therefore, for sheet specimens, in the potentials' range positively  $E_{i=0}^1 = -0.75$  V, stress-corrosion cracking proceeds by the mechanism of anodic dissolution; at potentials negatively -1.05 V – by the mechanism of hydrogen cracking. In the range of potentials from -0.75 to -1.05 V,

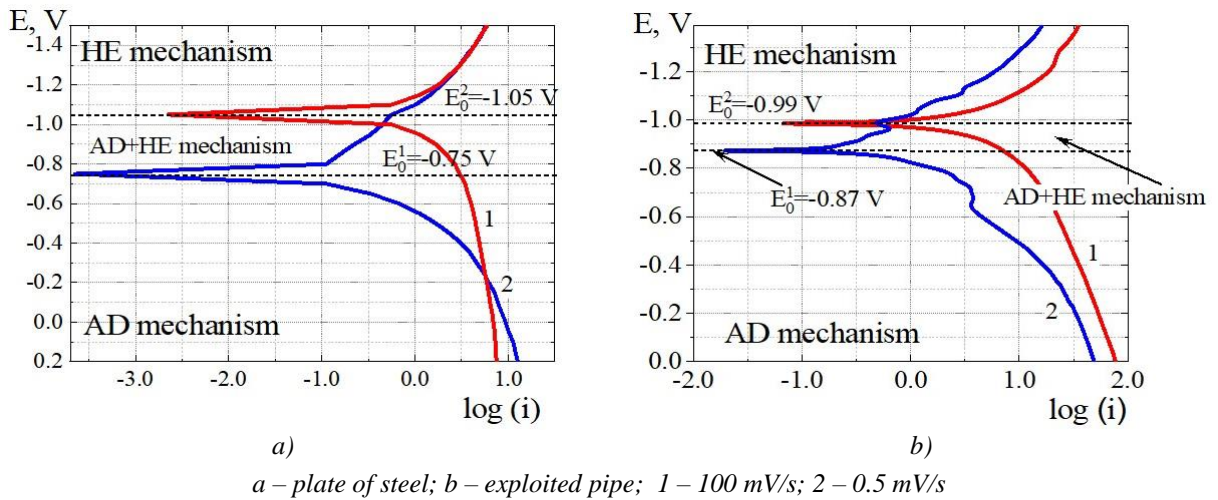


**Figure 7– Polarization curves of the steel specimens measured at high (100 mV/s) and low (0.5 mV/s) potential scanning rates in NS4 solution**

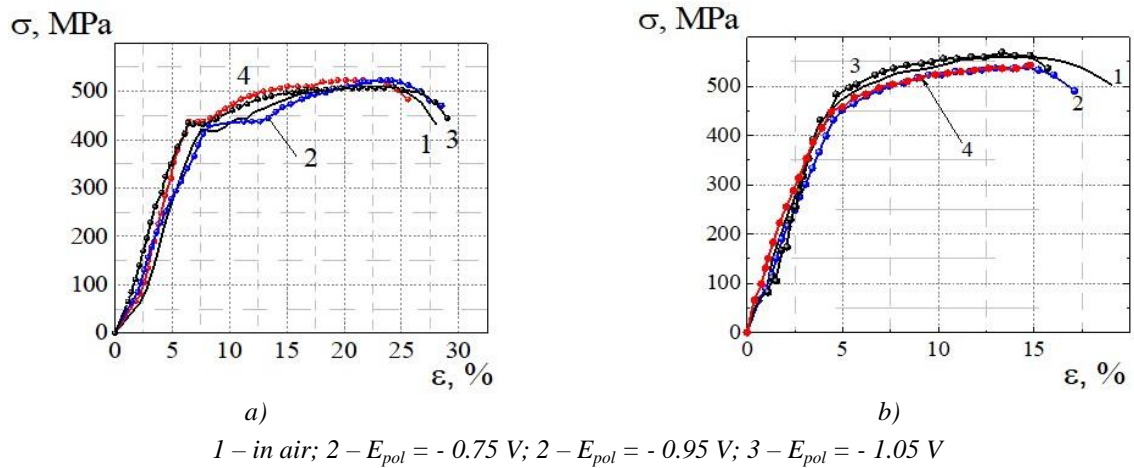


**Figure 8 – Destruction curves of X70 steel specimens in NS4 solution: steel sheet specimen (a) and a specimen of a long-term operated pipe (b)**

stress-corrosion cracking proceeds by a mixed mechanism: anodic dissolution and hydrogen embrittlement.

For specimens of the operated pipe, stress-corrosion cracking proceeds by the mechanism of anodic dissolution, at potentials more negative than -1.05 V by the mechanism of hydrogen embrittlement. In the range of potentials from -0.75 to -1.05 V, corrosion cracking proceeds by a mixed mechanism: anodic dissolution and hydrogen embrittlement.

It was determined that the width of the potential region in which stress-corrosion cracking occurs by a mixed mechanism is smaller for the operated pipe than for the steel sheet and equal to 120 and 300 mV, respectively (Fig. 7).

**Corrosion-mechanical and fractographic studies.**

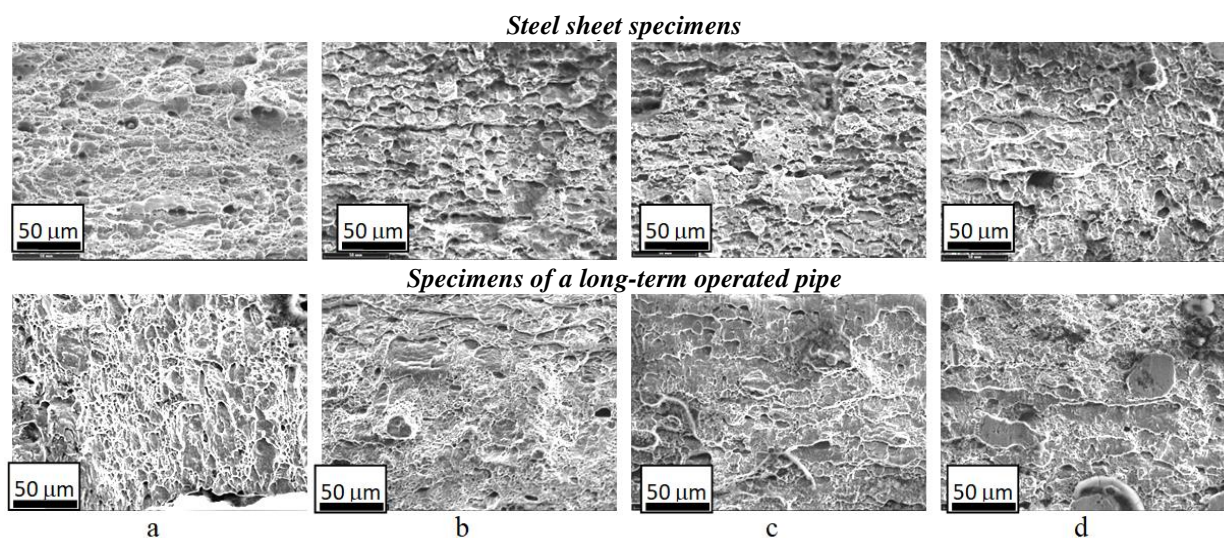
The destruction of the specimens from the sheet in the air occurred viscously; characteristic shrinkage near the place of rupture and the presence of areas that underwent plastic deformation are visible (Fig. 8). Relative elongation was 28 %, and relative narrowing was 73.8 % (Table 4). The morphology of the fracture is

viscous (dimpled in nature), and the size of the dimples mostly does not exceed 50 μm (Fig. 9, photo a).

At a minimum protective potential of -0.75 V, the destruction also occurred mainly viscously. A slight increase in relative elongation to 28.5 % and a decrease in relative narrowing to 69.4 % were observed (Table 4). The nature of the destruction, as in air, is viscous, but the increase in the size of the dimple and the decrease in their depth can be seen visually (Fig. 9, photo c).

At a potential of -0.95 V, the relative elongation was 29.0 % and the relative narrowing was 69.6 % (Table 4). The nature of the destruction, as in air, is viscous, but the increase in the size of dimples and the decrease in their depth can be seen visually (Fig. 9, photo c).

At the maximum protective potential of -1.05 V, an increase in the proportion of brittle part was noted in the fracture, the relative elongation decreased to 24.8 %, the relative narrowing reduced to 63.6 %, the coefficient of susceptibility to stress-corrosion cracking was 1.13 (Fig. 8, b, curve 3). On the fracture surface, almost flat areas of fracture of a larger area with a length of 10 to 30 μm prevail than on specimens destroyed at less negative potentials (Fig. 9, photo d).



a – in air, b –  $E_{pol} = -0.750\text{ V}$ , c –  $E_{pol} = -0.95\text{ V}$ , d –  $E_{pol} = -1.05\text{ V}$

**Figure 9 – SEM views of the morphology of fracture surface after breaking the steel specimens, cutting from a steel sheet specimen and a specimen of a long-term operated pipe at different conditions**

**Table 4 – Mechanical properties of X70 steel specimens of sheet and long-term operated pipe in air and in NS4 model soil electrolyte at different polarization potentials**

Tests conditions	$\delta, \%$	$S, \text{mm}^2$	$\psi, \%$	$K_S$	$C_0, \text{mol/m}^3$	$\delta, \%$	$S, \text{mm}^2$	$\psi, \%$	$K_S$	$C_0, \text{mol/m}^3$
	<i>Steel sheet specimens</i>					<i>Specimens of a long-term operated pipe</i>				
<b>Air</b>	28.0	7.90	73.8	—	—	19.1	8.79	70.7	0	—
<b>-0.75 V</b>	28.5	9.20	69.4	1.06	0	17.1	13.09	56.4	1.25	0
<b>-0.95 V</b>	29.0	9.12	69.6	1.06	0	15.7	14.23	52.6	1.35	0.019
<b>-1.05 V</b>	24.8	11.2	63.6	1.18	0.057	14.8	16.16	46.1	1.53	0.024

The coefficient of susceptibility to stress-corrosion cracking when the polarization potential changes in the range  $-0.75\text{ V} \rightarrow -0.95\text{ V} \rightarrow -1.05\text{ V}$  changed by  $1.06 \rightarrow 1.06 \rightarrow 1.18$ , respectively.

Viscous failure is characteristic of a pipe specimens after it breaks in air: shrinkage near the place of the break and the presence of areas that have undergone plastic deformation (Fig. 9). The relative elongation after rupture was 19.1 %, the cross-sectional area was 8.79 %, and the relative narrowing was 70.7 %. Pits of various sizes can be traced on the surface of the fracture; there are separate flat areas of brittle fracture (Fig. 9).

On the destruction curves in the solution under cathodic polarization, a decrease in the length of the descending curve sections was noted, which indicates a change in the nature of the destruction under the action of a corrosive environment and polarization. Stratification was found on the fracture surfaces of all specimens, which may be due to the applied steel manufacturing technology (in particular, controlled rolling).

The breakdown at the minimum protective potential of  $-0.75\text{ V}$  is viscous, the relative elongation and the relative contraction decreased to 17.1 and 56.4 %. The nature of the destruction, as in air, is viscous, but according to the visual assessment, it was

established that the share of brittle areas is no more than 10 % (Fig. 9).

At a potential of  $-0.95\text{ V}$ , there is a tendency to decrease for the fraction of viscous failure compared to air, a decrease in relative elongation to 15.7 % and relative narrowing to 52.6 %. On the surface of the fracture near one of the edges of the rupture, a long area with a flat nature of the fracture was found, which corresponds to (30–40) % of the area (Fig. 9).

On the specimens tested at the maximum protective potential of  $-1.05\text{ V}$ , the external signs of destruction are similar to those characteristic of the specimens destroyed at the potential of  $-0.95\text{ V}$ : the relative elongation and relative narrowing decreased to 14.8 and 46.1%. For this specimens, on the fracture surface, facets (elements of the fracture surface with clear boundaries lying in the same or close planes) of chipping were found, the share of the brittle fracture surface is approximately (20–30) % (Fig. 9).

The coefficient of susceptibility to stress-corrosion cracking of the operated pipe when the polarization potential changes in the range  $-0.75\text{ V} \rightarrow -0.95\text{ V} \rightarrow -1.05\text{ V}$  changed by  $1.25 \rightarrow 1.35 \rightarrow 1.53$ , respectively.

Thus, it was established that the specimens of a long-term operation under the conditions of comprehensive anti-corrosion protection of the main gas pipeline have an increased susceptibility to electrolytic

hydrogenation compared to the specimens made of steel sheet, and as a result, an increased susceptibility to stress-corrosion cracking.

### Conclusions

It was established that the concentration of hydrogen penetrating into steel during cathodic polarization for both types of specimens increases non-monotonically with a potential shift from -0.75 to -1.05 V: the hydrogenation of exploited steel specimens begins at a lower protective potential than for specimens of steel sheet: for -0.95 and -1.05 V, respectively. The concentration of hydrogen penetrating into steel for sheet specimens changes in the range  $0 \rightarrow 0 \rightarrow 0.057 \text{ mol/m}^3$ , for specimens from an operated pipe – in the range  $0 \rightarrow 0.019 \rightarrow 0.024 \text{ mol/m}^3$ .

It was determined that the electrochemical properties of both types of specimens change after electrolytic hydrogenation. While cathodic polarization potential is increasing in the series -0.75 V  $\rightarrow$  -0.95 V  $\rightarrow$  -1.05 V, for sheet steel specimens, the null current potential changes in the sequence -0.735 V  $\rightarrow$  -0.792 V  $\rightarrow$  -0.862 V, and for specimens of the operated pipe – in the series -0.738 V  $\rightarrow$  -0.719 V  $\rightarrow$  -0.704 V.

As a result of the hydrogen penetration process, an increase in susceptibility to stress-corrosion cracking of specimens from the operated pipe compared to specimens from sheet steel was observed. The coefficient of susceptibility to stress-corrosion cracking  $K_S$  for the steel sheet changed less intensively than for the specimens from the operated pipe, respectively: 1.06  $\rightarrow$  1.06  $\rightarrow$  1.18 and 1.25  $\rightarrow$  1.35  $\rightarrow$  1.53.

*The work was carried out with the support of the National Academy of Sciences of Ukraine 2019–2021, 2022 (state registration number of subjects 0118U100537, 0122U001188).*

### References

[1] Nyrkova, L & Osadchuk, S 2023, 'Stress-corrosion cracking of the steels of main gas pipeline: assessment and prevention', *Naukova dumka*, 216 p. <https://doi.org/10.15407/978-966-00-1845-7>

[2] Nyrkova, L 2020, 'Stress-corrosion cracking of pipe steel under complex influence of factors', *Engineering Failure Analysis*, vol. 116, 104757. <https://doi.org/10.1016/j.engfailanal.2020.104757>

[3] Laureys, A, Depraetere, R, Cauwels, M, Depover, T, Hertelé, S & Verbeken, K 2022, 'Use of existing steel pipeline infrastructure for gaseous hydrogen storage and transport: A review of factors affecting hydrogen induced degradation', *Journal of Natural Gas Science and Engineering*, 104534. <https://doi.org/10.1016/j.jngse.2022.104534>

[4] Shirband, Z, Shishesaz, MR & Ashrafi, A 2011, 'Hydrogen degradation of steels and its related parameters, a review', *Phase Transitions*, vol. 84, iss. 11–12, pp. 924–943. <https://doi.org/10.1080/01411594.2011.561774>

[5] Rybakov, AA, Goncharenko, LV, Filipchuk, TN, Lohman, IV & Burak, IZ 2014, 'Reasons of stress corrosion failure of erection girth joint of main gas pipeline', *The Paton*

*Welding Journal*, no. 3, pp. 49–52. <https://doi.org/10.15407/tpwj2014.03.09>

[6] Polyakov, SG & Rybakov, AA 2009, 'The main mechanisms of stress corrosion cracking in natural gas trunk lines', *Strength of Materials*, no. 41, pp. 456–463. <https://doi.org/10.1007/s11223-009-9164-x>

[7] Nyrkova, L, Rybakov, A, Goncharenko, L, Osadchuk, S & Kharchenko, Yu 2023, 'Analysis of the causes of fracture of the main gas pipeline', *Zaštita materijala*, vol. 64, no. 2, pp. 177–189. <https://doi.org/10.5937/zasmat2302177N>

[8] Lu, WC & Wu, JK 1996, 'The influence of microstructure on hydrogen transport in carbon steels', *Corrosion Science*, vol. 38, pp. 239–245. [https://doi.org/10.1016/0010-938X\(96\)00109-6](https://doi.org/10.1016/0010-938X(96)00109-6)

[9] Dey, S, Mandhyan, AK, Sondhi, SK & Chattoraj, I 2006, 'Hydrogen entry into pipeline steel under freely corroding conditions in two corroding media', *Corrosion Science*, vol. 48, pp. 2676–2688. <https://doi.org/10.1016/j.corsci.2005.10.003>

[10] Lu, BT, Luo, JL, Norton, PR & Ma, HY 2009, 'Effects of dissolved hydrogen and elastic and plastic deformation on active dissolution of pipeline steel in anaerobic groundwater of near-neutral Ph', *Acta Materialia*, vol. 57, pp. 41–49.

[11] Meng, GZ, Zhang, C & Cheng, YF 2008, 'Effects of corrosion product deposit on the subsequent cathodic and anodic reactions of X-70 steel in near-neutral pH solution', *Corrosion Science*, vol. 50, pp. 3116–3122. <https://doi.org/10.1016/j.corsci.2008.08.026>

[12] Nykyforchyn, HM 2011, 'Specific features of hydrogen-induced corrosion degradation of steels of gas and oil pipelines and oil storage reservoirs', *Materials Science*, vol. 47, pp. 127–136. <https://doi.org/10.1007/s11003-011-9390-9>

[13] Kryzhanivskiy, YeI & Nykyforchyn, HM 2013, 'Corrosion-hydrogen degradation of gas transport systems', *Scientific Notes*, vol. 41, iss. 1, pp. 148–153.

[14] Paton, BE, Semenov, SE, Rybakov, AA, Vasilenko, SK & Vasilyuk, VM 2000, 'Ageing and procedure of evaluation of the state of metal of the main pipelines in service', *The Paton welding journal*, no. 7, pp. 2–20.

[15] Semenov, SE, Rybakov, AA, Kirian VI, Filipchuk, TN, Goncharenko, LV, Vasilyuk, VM & Vlasyuk, FS 2001, 'Experimental evaluation of the state of metal of long-serviced welded oil pipelines', *The Paton welding journal*, no. 5, pp. 17–21.

[16] Semyonov, SE, Rybakov, AA, Goncharenko, LV, Filipchuk, TN, Drogomiretsky, MN & Pedko, BI 2003, 'Evaluation of condition of metal of welded pipes of long-operated gas pipelines', *The Paton welding journal*, no. 4, pp. 2–6.

[17] Nyrkova, LI, Goncharenko, LV, Rybakov, AO, Osadchuk, SO, Klymenko, AV, & Kharchenko, YuO 2023, 'Investigation of welded joints of long-term operated gas pipeline controllable rolled X70 steel', *FME Transactions*, vol. 51, iss. 1, pp. 71–80. <https://doi.org/10.5937/fme2301071N>

[18] Rahman, KMM, Qin, W, Szpunar, JA, Kozinski, J, Song, M & Zhu, N 2021, 'New insight into the role of inclusions in hydrogen-induced degradation of fracture toughness: three-dimensional imaging and modeling', *Philosophical Magazine*, vol. 101, iss. 8, pp. 976–996. <https://doi.org/10.1080/14786435.2021.1876267>

[19] Peng, Z, Cao, C, Huang, F, Wang, L, Xue, Z & Liu, J 2023, 'Effect of slow strain rates on the hydrogen migration and different crack propagation modes in pipeline steel', *Steel research international*, First published: 11 March. <https://doi.org/10.1002/srin.202300070>

- [20] Kryzhanivskiy, YeI 2014, 'Degradation of materials of oil and gas facilities in long-term operation and ways to ensure their operability', *Development of deposits: Collection of sci. works*, vol. 8, pp. 241–253.
- [21] Krechkovska, HV, Tsyurulnyk, OT & Student, OZ 2019, 'In-Service Degradation of Mechanical Characteristics of Pipe Steels in Gas Mains', *Strength Materials*, vol. 51, pp. 406–417. <https://doi.org/10.1007/s11223-019-00087-4>
- [22] Zvirko, OI 2021, 'In-Service Degradation of Structural Steels (A Survey)', *Materials Sciences*, vol. 57, pp. 319–330. <https://doi.org/10.1007/s11003-021-00547-w>
- [23] Maruschak, PO, Danyliuk, IM, Bishchak, RT et al. 2014, 'Low temperature impact toughness of the main gas pipeline steel after long-term degradation', *Central European Journal of Engineering*, vol. 4, pp. 408–415. <https://doi.org/10.2478/s13531-013-0178-6>
- [24] Cheng, YF 2013, *Stress corrosion of pipeline* / edited by R. Winston. New Jersey, John Wiley & Sons Inc., 288 p.
- [25] Technical Specification 14-3-995–81. Expanded electric-welded longitudinally welded steel pipes with a diameter of 1420 mm from X70 grade steel.
- [26] R. Antunes de Sena, I. Napoleão Bastos, G. Mendes Platt, 2012. Theoretical and Experimental Aspects of the Corrosivity of Simulated Soil Solutions, *International Scholarly Research Notices*. Article ID 103715, 6 pages.
- [27] GOST R 9.915–2010. Unified system of corrosion and ageing protection. Metals, alloys, coatings, products. Test methods of hydrogen embrittlement]. Moscow, Standartinform Publ., 2011, 31 p. [in Russian]
- [28] GOST 5640-68 Steel. Metallographic method for determination of microstructure of sheets and bands. [in Russian]
- [29] DSTU 8972:2019 Steel and alloys. Methods for detection and determination of grain size. [in Ukrainian]
- [30] Nyrkova, LI, Klymenko, AV, Osadchuk, SO & Kovalenko, SYu 2023, 'Comparative investigation of electrolytic hydrogenation of pipe assortment steel under cathodic polarization', *International Journal of Hydrogen Energy*, Available online 12 July 2023. <https://doi.org/10.1016/j.ijhydene.2023.06.316>
- [31] Liu, ZY, Li, XG & Cheng, YF 2010, 'In-situ characterization of the electrochemistry of grain and grain boundary of anX70 steel in a near-neutral pH solution', *Electrochem. Commun.*, vol. 12, p. 936–938. <https://doi.org/10.1016/j.elecom.2010.04.025>

УДК 620.197.5:620.194.22

## Вплив електролітичного наводнювання на корозійне розтріскування сталі X70 та труби тривалоексплуатованого магістрального газопроводу

<sup>1</sup>Л. І. Ниркова, <sup>1</sup>А. В. Клименко, <sup>1</sup>Л. В. Гончаренко, <sup>1</sup>С. О. Осадчук,  
<sup>1</sup>С. Ю. Коваленко, <sup>1</sup>Ю. О. Харченко, <sup>2</sup>В. В. Лавренюк

<sup>1</sup>Інститут електрозварювання ім. Є. О. Патона НАН України;  
вул. Казимира Малевича, 11, м. Київ, 03150, Україна

<sup>2</sup>Київський національний університет технологій та дизайну;  
вул. Мала Шияновська (Немировича-Данченка), 2, м. Київ, 01011, Україна

Катодна поляризація, яка застосовується при комплексному протикорозійному захисті магістральних газопроводів для зниження швидкості корозії до технічно допустимого рівня викликає розклад ґрунтового електроліту з відновленням водню, а його проникнення в сталь за дії розтягових напружень сприяє зміні механічних властивостей труб та опірності корозійному розтріскуванню. Проведено комплексні дослідження та визначено вплив електролітичного наводнювання на корозійне розтріскування зразків сталі категорії міцності X70, виготовлених зі сталевих листа та труби тривалоексплуатованого магістрального газопроводу, у модельному ґрунтовому електроліті NS4 за катодної поляризації в діапазоні потенціалів від -0.75 до -1.05 В. У роботі застосовували такі методи: деформації з малою швидкістю, потенціометрії, вольтамперометрії, електролітичного наводнювання, метод сканувальної електронної мікроскопії, оптичної мікроскопії. Встановлено, що для обох видів зразків концентрація водню, що проникає в сталь при катодній поляризації, немонотонно зростає із зменшенням потенціалу від -0.75 до -1.05 В. Відзначено, що наводнювання зразків експлуатованої сталі починається за нижчого захисного потенціалу, ніж зразків зі сталевих листа: за -0.95 та -1.05 В, відповідно. Концентрація водню, що дифундує в сталь, для зразків з листа змінюється в ряду  $0 \rightarrow 0 \rightarrow 0.057$  моль/м<sup>3</sup>, для зразків з експлуатованої труби –  $0 \rightarrow 0.019 \rightarrow 0.024$  моль/м<sup>3</sup>. Як наслідок перебігу процесу дифузії водню відбувається підвищення схильності до корозійного розтріскування зразків з експлуатованої труби порівняно із зразками з листової сталі. Коефіцієнт схильності до корозійного розтріскування  $K_S$  для листа зі сталі змінюється менш інтенсивно, ніж для зразків з експлуатованої труби:  $1.06 \rightarrow 1.06 \rightarrow 1.18$  та  $1.25 \rightarrow 1.35 \rightarrow 1.53$ , відповідно. Отже, встановлено підвищення схильності до електролітичного наводнювання зразків, виготовлених з труби тривалоексплуатованого в умовах комплексного протикорозійного захисту магістрального газопроводу порівняно із зразками зі сталевих листа, і як наслідок – підвищення схильності до корозійного розтріскування.

Ключові слова: деформація з малою швидкістю, електролітичне наводнювання, корозійне розтріскування, потенціометрія, сканувальна електронна мікроскопія.